IEEE Photonics Journal
An IEEE Photonics Society Publication

Linearity Characterization of a Dual–Parallel Silicon Mach–Zehnder Modulator

Volume 8, Number 6, December 2016

Yanyang Zhou
Linjie Zhou, *Member, IEEE*
Minjuan Wang
Yujie Xia
Yiming Zhong
Xinwan Li, *Senior Member, IEEE*
Jianping Chen

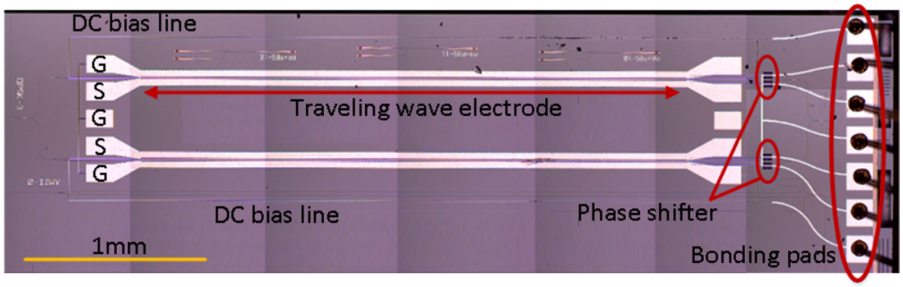

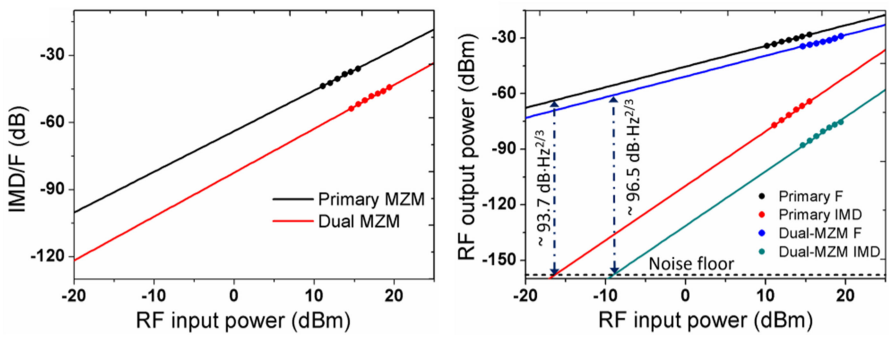

DOI: 10.1109/JPHOT.2016.2616488
1943-0655 © 2016 IEEE

Linearity Characterization of a Dual–Parallel Silicon Mach–Zehnder Modulator

Yanyang Zhou, Linjie Zhou, *Member, IEEE*, Minjuan Wang, Yujie Xia, Yiming Zhong, Xinwan Li, *Senior Member, IEEE*, and Jianping Chen

State Key Laboratory of Advanced Optical Communication Systems and Networks, Department of Electronic Engineering, Shanghai Jiao Tong University, Shanghai 200240, China

DOI:10.1109/JPHOT.2016.2616488

Manuscript received September 7, 2016; revised October 3, 2016; accepted October 5, 2016. Date of publication October 12, 2016; date of current version October 27, 2016. This work was supported in part by the National Natural Science Foundation of China under Grant 61422508, Grant 61535006, and Grant 61661130155. Corresponding author: L. Zhou (e-mail: ljzhou@sjtu.edu.cn).

Abstract: We report a high-linearity wideband dual–parallel silicon Mach–Zehnder modulator (MZM). This modulator consists of two carrier-depletion-based MZMs with a single-drive push–pull traveling wave electrode configuration. An analytic model is established to investigate the linearity property of the modulator. The measurement results show the modulator can effectively suppress third-order harmonics and third-order intermodulation distortions, with improved modulation linearity, compared to a single MZM.

Index Terms: Silicon modulator, microwave photonics, integrated optics devices.

1. Introduction

Silicon photonic integration is one of the most attractive platforms for microwave photonic (MWP) links due to its low cost, high energy efficiency, and compactness. An optical modulator converts radio-frequency (RF) signal from the electrical domain to the optical domain. One of the most important performance metrics is its linearity [1], [2]. The carrier-depletion-based silicon Mach-Zehnder modulator (MZM) exhibits high performances in terms of modulation speed and power consumption [3]–[6]. However, it has an inherent nonlinear transfer function, which limits the spur-free dynamic range (SRDR) due to the harmonic and intermodulation distortions [7]. Ring-assisted Mach-Zehnder Interferometer (RAMZI) modulators [8] and dual-parallel MZMs [9], [10] have been proposed as two effective approaches to linearize the transfer function and reduce the distortion. The linearized RAMZI modulator based on the free carrier dispersion effect has been presented in [11], which utilizes the phase response of a ring resonator to cancel the nonlinear phase response of the MZM. The challenge with this approach is that the ring resonator coupling coefficient needs to be well adjusted to cancel the distortion completely. In the dual-parallel MZM, the linearity is improved when the two MZMs are driven with different RF signal magnitudes and fed with different optical powers so that the distortions induced by the two MZMs counteract each other. The dual-parallel MZM is superior to the RAMZI as it has a boarder optical bandwidth and higher tolerance to fabrication and temperature variations.

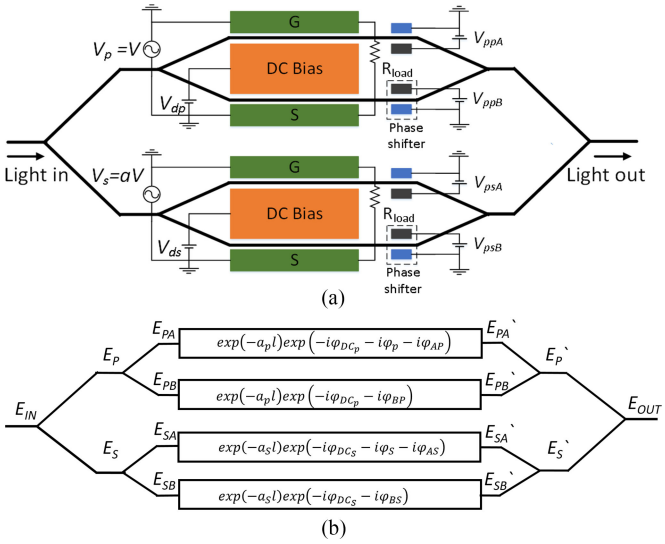

Fig. 1. (a) Schematic structure of the dual-parallel silicon MZM. (b) Analytic model of the dual-parallel MZM.

In this paper, we characterize the modulation linearity of a dual-parallel silicon MZM with single-drive push-pull travelling wave electrodes (TWEs). A theoretical model is established to analyze the device linearity performance. The measurement results show that the third-order harmonic term is significantly reduced by using the dual-parallel MZM. In addition, under the same input RF power, the ratio of the third-order intermodulation distortion (IMD) to the fundamental tone is decreased considerably.

2. Analytic Model

Fig. 1(a) shows the schematic structure of the dual-parallel silicon MZM. The MZM is composed of two nested carrier-depletion-based single-drive push-pull MZMs. The single-drive push-pull configuration has the merits of low chirp, low loading capacitance and simplified RF connection interface [12]. The TWE is 3-mm-long and has been optimized to achieve impedance match and velocity match [13]. The RF signal is applied onto the TWE connected to the heavily p-type doped regions, and a DC bias is applied to the heavily n-type doped region in the MZI center. Each child MZM contains two 50-μm-long thermo-optic (TO) phase shifters [14]. The optical power splitters/combiners in the MZMs are implemented by 1 x 2 and 2 x 1 multimode interference (MMI) couplers. The top child MZM works as the primary modulator with its bias at a quadrature point and the bottom child MZM works as the secondary modulator with its bias at another quadrature point π-phase-different from the primary modulator (the two child modulators are denoted by the subscript *p* and *s*). The input optical power is higher in the primary modulator while its RF drive power is lower than the secondary modulator. In this way, by properly choosing the ratios of both the input optical power and the RF power for the two modulators, the third-order distortions of the primary and secondary modulators can be cancelled, while the fundamental signal power only suffers a slight reduction. In order to explain the linearization process of this approach, an analytic model is established using the optical field transfer functions as shown in Fig. 1(b).

The input optical power is denoted as P_{in}, and the corresponding field amplitude is denoted as E_{in}. The output of the primary MZM and the secondary MZM are coherently recombined. Then, the electrical current produced in a square-law detector is proportional to the output power, which is given by

$$P_{out} = |E_{out}|^2 = \frac{1}{2}\left(E_p^{`} + E_s^{`}\right)\left(E_p^{`} + E_s^{`}\right)^*. \quad (1)$$

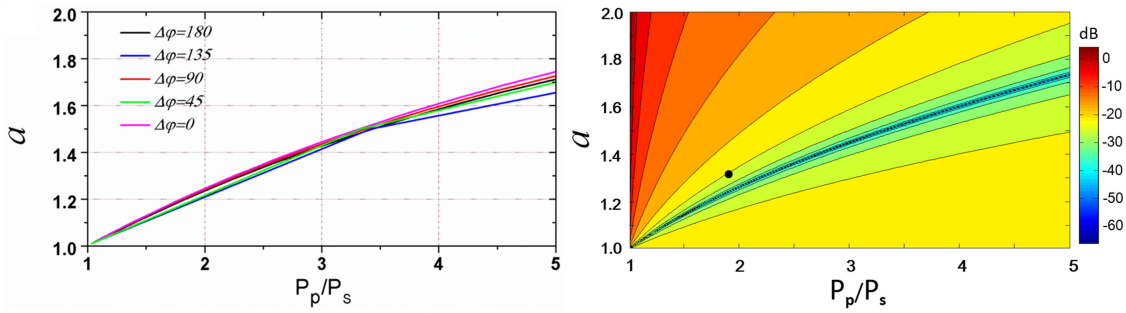

Fig. 2. (a) Values of P_p/P_s and a to get $P_3 = 0$ under various $\Delta\varphi$. (b) Ratio of P_3/P_1 when $\Delta\varphi = 0$ and $V = 0.1V_\pi$. The dot represents the values used in the measurement.

Assuming that the two arms of each child MZM have identical PN junctions, we denote the phase changes caused by the DC bias and RF signal as φ_{DCp}, φ_{Ap}, and φ_{Bp} for the primary MZM and φ_{DCs}, φ_{As}, and φ_{Bs} for the secondary MZM, respectively. The field loss factor for the two child MZMs is represented by $a_{p,s}$. The phase difference between the two arms of the two child MZMs is represented by $\varphi_{p,s}$, which is set by the TO phase shifters. In a push-pull configuration, the top and bottom arms are subject to opposite RF drive voltages, and therefore, the phase modulation of the top and bottom arms of the two MZMs, respectively, satisfies

$$\begin{aligned} \varphi_{Ap} - \varphi_{Bp} &= \pi V/V_\pi \\ \varphi_{As} - \varphi_{Bs} &= \pi aV/V_\pi \end{aligned} \tag{2}$$

where V and aV ($a > 1$) are drive voltages applied on the primary and secondary MZMs, respectively. Thus, the output power can be written as

$$\begin{aligned} P_{out} = \frac{1}{2}\Bigg[P_p + P_s + P_p\cos\left(\varphi_p + \pi\frac{V}{V_\pi}\right) + P_s\cos\left(\varphi_s + \pi\frac{aV}{V_\pi}\right) \\ + 4\sqrt{P_pP_s}\cos(\Delta\varphi)\cos\left(\frac{\varphi_p}{2}\right)\cos\left(\frac{\varphi_s}{2} + \pi\frac{a-1}{2V_\pi}V\right)\Bigg] \end{aligned} \tag{3}$$

$$P_p = P_{in}\exp\left(-2a_pl\right)/4 \tag{4}$$

$$P_s = P_{in}\exp\left(-2a_sl\right)/4 \tag{5}$$

$$\Delta\varphi = \varphi_{DCp} - \varphi_{DCs} + \left(\varphi_p - \varphi_s\right)/2\,. \tag{6}$$

We assume the two child MZMs work at the opposite quadrature points ($\varphi_p = \pi/2$, $\varphi_s = 3\pi/2$). With Taylor series expansion of (3), the output power can be written as the summation of the constant (P_0), linear (P_1), quadratic (P_2) and cubic (P_3) terms:

$$P_{out} = P_0 + P_1(V) + P_2(V^2) + P_3(V^3) \tag{7}$$

where

$$P_0 = \frac{1}{2}P_p + \frac{1}{2}P_s - \sqrt{P_pP_s}\cos(\Delta\varphi) \tag{8}$$

$$P_1 = \frac{1}{2}\left[-P_p\left(\pi\frac{V}{V_\pi}\right) + P_s\left(\pi\frac{aV}{V_\pi}\right) - \sqrt{P_pP_s}\cos(\Delta\varphi)\left(\pi\frac{a-1}{V_\pi}V\right)\right] \tag{9}$$

$$P_2 = \frac{1}{8}\sqrt{P_pP_s}\cos(\Delta\varphi)\frac{(a-1)^2V^2\pi^2}{V_\pi^2} \tag{10}$$

$$P_3 = P_p\frac{V^3\pi^3}{12V_\pi^3} - P_s\frac{a^3V^3\pi^3}{12V_\pi^3} + \frac{1}{48}\sqrt{P_pP_s}\cos(\Delta\varphi)\frac{(a-1)^3V^3\pi^3}{V_\pi^3} \tag{11}$$

It can be seen that P_3 is a function of P_p, P_s, a, and $\Delta\varphi$. Therefore, it is possible to eliminate P_3 by choosing a proper set of parameters. We remark that when P_3 is eliminated, both the third-order harmonic and the third-order IMD are removed. Fig. 2(a) shows the relationship between P_p/P_s and a at various $\Delta\varphi$ values to get $P_3 = 0$. It should be noted that P_1 is also reduced when P_3 is completely eliminated. The reduction reaches the minimum when $\Delta\varphi = 0$ as seen from (9). Fig. 2(b) shows the power ratio (in dB unit) of the cubic relative to the linear term $10\log_{10}|P_3/P_1|$, where $\Delta\varphi = 0$, and the RF voltage $V = 0.1V_\pi$. It can be seen, in order to suppress the third-order distortion, that it is better to set the values of P_p/P_s and a near the blue region.

When the operation point of the MZM is at the quadrature, the second-order nonlinear term coming from the MZM transfer function can be eliminated. However, for the carrier-depletion-based silicon MZM, the second-order harmonics are also generated by the nonlinear optical loss and phase shift [7]. Therefore, it is difficult to completely eliminate the second order harmonic for the primary MZM. According to (10), the quadratic term P_2 for the dual-parallel MZM can be removed by making $a = 1$. However, as shown in Fig. 2(b), the third-order IMD and the second-order distortion cannot be eliminated simultaneously. Our work mainly concentrates on reducing the third-order IMD since the second-order harmonic is far from the fundamental tone and can be easily eliminated by filtering in practical systems.

3. Experimental Results

Fig. 3(a) shows the experimental setup to measure the linearity of the dual-parallel MZM. The RF signal generated by the microwave generator (R&S SMB100A) or the vector network analyzer (VNA, PNA-X N5247A) was used to measure the third-order harmonic component and the IMD, respectively. It was divided into two paths and amplified by two RF amplifiers. Different a values can be obtained by adjusting the gain of the two RF amplifiers. The RF signals were fed into the dual-parallel MZM via a 40-GHz-bandwidth microwave GSGSG probe. The other ends of the TWEs were terminated with two external 50-Ω resistors via another GSGSG probe. The ratio P_p/P_s can be varied by applying different DC biases to the two MZMs. The operation point of each MZM was set by the TO phase shifters. Input light from a continuous wave tunable laser (TL, TSL-710) with the transverse electric (TE) polarization set by the polarization controller (PC) was coupled to the MZM through an on-chip inverse taper. The output signal was amplified by an erbium-doped fiber amplifier (EDFA) followed by an optical filter before received by a photodiode (PD) with a responsivity of 0.5 A/W. The converted electrical signal was finally fed back to the electrical spectrum analyzer (ESL, R&S FSUP50) or VNA for RF spectrum and linearity measurements, respectively. The device was fabricated using the IME standard CMOS process. Fig. 3(b) shows the image of the fabricated device after wire-bonding to a printed circuit board (PCB). The footprint of our device is 4.77 mm $\times$ 1.35 mm. The DC bias and phase shifter electrical lines were connected to a PCB through wire bonding.

The optical insertion loss of the dual-parallel-MZM is about 15 dB, including 8 dB coupling loss, 6 dB waveguide loss and 1 dB loss from the MMI splitters and combiners. With the increased DC bias applied onto the MZM, the depletion region of the PN junction keeps broadening, which reduces the optical loss from the free-carrier absorption. Fig. 4(a) shows the measured reduction of optical loss and the phase shift as a function of bias voltage for the MZM. Therefore, P_p/P_s can be varied by applying different bias voltages onto the two child MZMs. It should be noted that the maximum loss reduction is about 3.2 dB, which limits the maximum P_p/P_s. The π phase shift can be obtained at 5 V bias for the 3 mm-long modulation arm, and therefore, the modulation efficiency is $V_\pi L = 1.5\,V \cdot cm$. The TO phase shifters were optimized to achieve a high thermal efficiency. Fig. 4(b) shows the phase change as a function of voltage for the TO phase shifter. Fig. 4(c) shows the measured S_{21} parameters under different bias voltages. A large bias voltage can decrease the RF loss of the TWE. Fig. 4(d) shows the measured electro-optical (EO) modulation response of the MZM with the input optical wavelength tuned to set the modulator at the quadrature point. The measured EO 3-dB bandwidth is 16 GHz at $V_d = 0\,V$ and increases to 30 GHz at $V_d = 6\,V$. It can

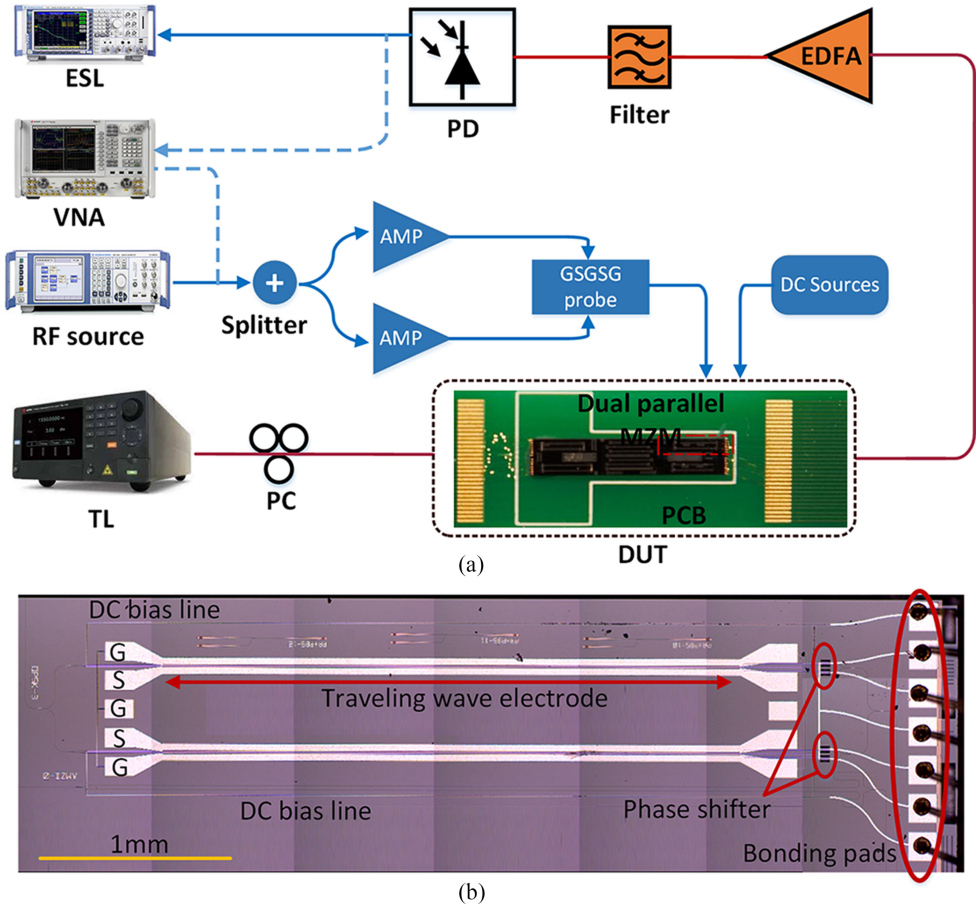

Fig. 3. (a) Experimental setup to measure the linearity of the dual-parallel MZM. (b) Microscope image of the MZM.

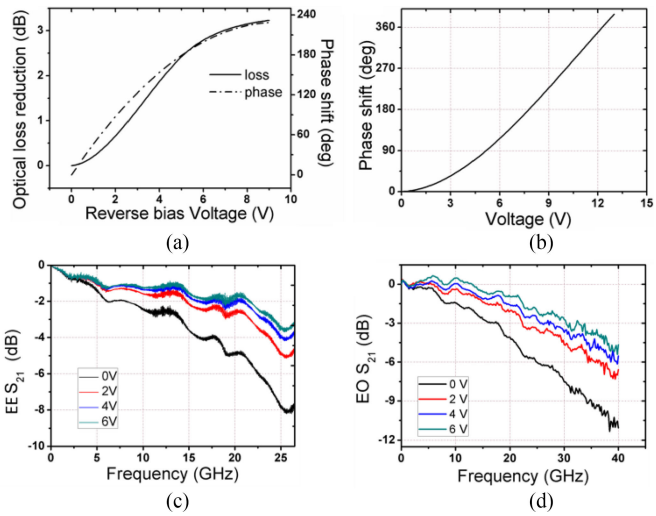

Fig. 4. (a) Optical loss reduction and phase shift versus reverse bias voltage. (b) Phase change as a function of voltage for the TO phase shifters. (c) EE S_{21} and (d) EO S_{21} responses under various DC biases.

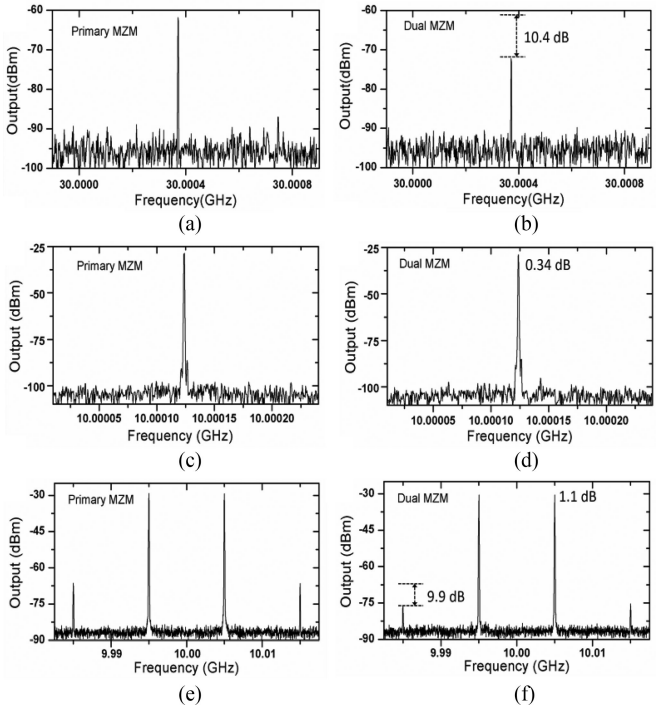

Fig. 5. (a)–(d) Output RF spectra showing the fundamental and the third-order harmonic tones measured by the ESL. (a) and (b) Third-order harmonic tone. (c) and (d) Fundamental tone. (e) and (f) Output RF spectra of the fundamental and the IMD measured by the VNA.

be seen that when $V_d > 2$ V, the dual-MZM exhibits a flat EO response from DC to 15 GHz, which is suited for the microwave photonics applications.

To measure the high-order harmonics, a 10 GHz RF signal generated by the microwave generator was used to drive the modulator. According to Fig. 4(a), when the primary MZM is biased at $V_{dp} = 9$ V and the secondary MZM is biased at $V_{ds} = 1.7$ V, P_p is 2.73 dB larger than P_s, and thus P_p/P_s is 1.87. The modulation operation point was set by tuning the phase shifters in each MZM. The primary MZM was operated at $\pi/2$ when $V_{ppA} = 5.2$ V and $V_{ppB} = 0$ V; the secondary MZM was operated at $3\pi/2$ when $V_{psA} = 3.5$ V and $V_{psB} = 11.2$ V. The RF signal powers applied on the primary and secondary MZMs were 14.55 dBm and 16.3 dBm, respectively ($a = 1.25$). Fig. 5(a)–(d) compare the RF spectra of the fundamental and the third-order harmonic for the primary MZM only (no RF signal on the slave MZM) and the dual-parallel MZM. It can be seen that the third-order harmonic tone of the dual-parallel MZM is reduced by about 10.4 dB, while the fundamental tone only suffers about a 0.34 dB reduction.

The third-order IMD is regarded as the major limiting distortion factor in the MWP links. Because this frequency component falls close to the fundamental component, which could hardly be filtered out in practice. For the IMD measurement, a two-tone RF signal was generated by the VNA with the frequencies at 9.995 GHz and 10.005 GHz. The RF spectra in Fig. 5(e) and (f) illustrate the relative magnitude of the fundamental and the IMD. Compared to the primary MZM, the fundamental tone of the dual-parallel MZM is only lowered by about 1.1 dB, while the IMD is suppressed by 9.9 dB. As indicated by Fig. 2(b), a smaller a can further reduce the IMD. However, the fundamental tone will also suffer a larger power reduction. The measurement result on overall matches the theoretical prediction. The discrepancy lies in the fact that the nonlinearities of the PN junction and the optical loss were not taken into consideration in the analytical model [7].

Fig. 6(a) shows the measured IMD to fundamental ratio (IMD/F) versus RF input power for the primary and the dual-parallel MZMs. The RF input power of the dual-parallel MZM is the summation of the RF power applied onto the primary and secondary MZMs. Comparing the two

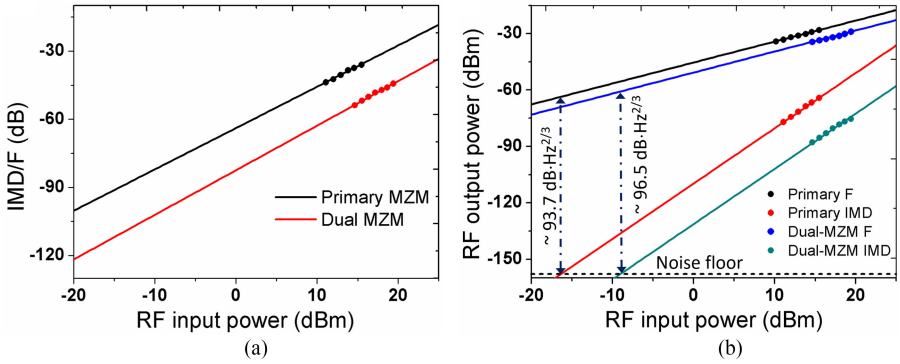

Fig. 6. (a) IMD to fundamental ratio versus input RF power for the primary and dual-parallel MZMs with the RF frequencies at 9.995 GHz and 10.005 GHz. (b) Measured SFDR of the primary MZM and the dual-parallel MZM. Solid lines are the linear fitting lines.

TABLE 1
Modulator Linearity Comparison

Ref.	Device	Received power (mW)	Noise floor (dBm/Hz)	$SFDR_{IMD}$ ($dB \cdot Hz^{2/3}$)
[15]	Ring	20	−163	84@1 GHz
[16]	Ring	1	−148	87.6@10 GHz
[17]	MZI	0.8	−160	90@5 GHz
[6]	MZI	1	−165	97@1 GHz
[11]	RAMZI	5.9	−161	99@10 GHz
[18]	Dual-parallel MZM	2	−122	86@10 GHz
This work	Dual-parallel MZM	2	−157	96.5@10 GHz

traces, the IMD/F is reduced by about 17 dB for the dual-parallel MZM at the same RF input power. The noise floor measured by the ESL is –147dB with a 10 Hz resolution bandwidth (–157 dB in the bandwidth of 1 Hz), mainly limited by the noise figure of EDFA. The optical power received by the photodetector is 3 dBm. Compared to the primary MZM, the $SFDR_{IMD}$ of the dual-parallel MZM is $\sim 96.5\,dB \cdot Hz^{2/3}$ with 2.9 dB improvement, as shown in Fig. 6(b).

Finally, we compare our device with the silicon modulators reported in the literature [6], [11], [15]–[18], as shown in Table 1. The linearity of silicon ring modulator can be improved by using $LiNbO_3$ as the electro-optical medium to avoid the nonlinearity of silicon plasma dispersion effect, but the fabrication is relatively complicated [16]. The single MZM exhibits $SFDR_{IMD}$ of 97 $dB \cdot Hz^{2/3}$ near 1GHz in [6]. However, the input optical power is as high as 500 mW. Compared with the RAMZI modulator, our device presents a high $SFDR_{IMD}$ at 10 GHz with a lower received power and a higher noise floor. A higher SFDR could be achieved by lowering the noise floor in the optical link and reducing the coupling loss.

4. Conclusion

We have characterized the linearity of a dual-parallel silicon MZM with single-drive push-pull TWEs. A theoretical model has been established, and it reveals that the linearity can be improved by properly adjusting the RF power, the bias voltage, and the operation point of the primary and the

secondary MZMs. The measurement results show the IMD can be suppressed by about 9.9 dBm, while the fundamental tones only reduced by 1.1 dBm at 10 GHz for the dual-parallel MZM compared to the primary MZM only. This results in a 2.9 dB improvement in $SFDR_{IMD}$. A larger P_p/P_s can be obtained by incorporating a VOA into the slave MZM so that the third-order harmonic can be further suppressed to give a lower IMD.

References

[1] D. Marpaung, C. Roeloffzen, R. Heideman, A. Leinse, S. Sales, and J. Capmany, "Integrated microwave photonics," *Laser Photon. Rev.*, vol. 7, no. 4, pp. 506–538, 2013.

[2] Y. Pan *et al.*, "Adaptive linearized microwave downconversion utilizing a single dual-electrode Mach–Zehnder modulator," *Opt. Lett.*, vol. 40, no. 11, pp. 2649–2652, Jun. 2015.

[3] P. Dong, L. Chen, and Y.-k. Chen, "High-speed low-voltage single-drive push-pull silicon Mach-Zehnder modulators," *Opt. Exp.*, vol. 20, no. 6, pp. 6163–6169, Mar. 2012.

[4] H. Xu *et al.*, "High-speed silicon modulator with band equalization," *Opt. Lett.*, vol. 39, no. 16, pp. 4839–4842, Aug. 2014.

[5] T. Li *et al.*, "Low-voltage, high speed, compact silicon modulator for BPSK modulation," *Opt. Exp.*, vol. 21, no. 20, pp. 23410–23415, Oct. 2013.

[6] M. Streshinsky *et al.*, "Highly linear silicon traveling wave Mach-Zehnder carrier depletion modulator based on differential drive," *Opt. Exp.*, vol. 21, no. 3, pp. 3818–3825, Feb. 2013.

[7] A. Khilo, C. M. Sorace, and F. X. Kärtner, "Broadband linearized silicon modulator," *Opt. Exp.*, vol. 19, no. 5, pp. 4485–4500, Feb. 2011.

[8] X. Xie, J. Khurgin, J. Kang, and F.-S. Chow, "Linearized Mach-Zehnder intensity modulator," *IEEE Photon. Technol. Lett.*, vol. 15, no. 4, pp. 531–533, Apr. 2003.

[9] J. L. Brooks and R. Becker, "Implementation and evaluation of a dual parallel linearization system for AM-SCM video transmission," *J. Lightw. Technol.*, vol. 11, no. 1, pp. 34–41, Jan. 1993.

[10] S. K. Korotky and R. M. De Ridder, "Dual parallel modulation schemes for low-distortion analog optical transmission," *IEEE J. Sel. Areas. Commun.*, vol. 8, no. 7, pp. 1377–1381, Sep. 1990.

[11] J. Cardenas *et al.*, "Linearized silicon modulator based on a ring assisted Mach Zehnder inteferometer," *Opt. Exp.*, vol. 21, no. 19, pp. 22549–22557, Sep. 2013.

[12] L. Chen, P. Dong, and Y. K. Chen, "Chirp and dispersion tolerance of a single-drive push-pull silicon modulator at 28 Gb/s," *IEEE Photon. Technol. Lett.*, vol. 24, no. 11, pp. 936–938, Jun. 2012.

[13] Y. Zhou *et al.*, "Modeling and optimization of a single-drive push pull silicon Mach Zehnder modulator," *Photon. Res.*, vol. 4, no. 4, pp. 153–161, Aug. 2016.

[14] Q. Wu, L. Zhou, X. Sun, H. Zhu, L. Lu, and J. Chen, "Silicon thermo-optic variable optical attenuators based on Mach–Zehnder interference structures," *Opt. Commun.*, vol. 341, pp. 69–73, Dec. 2015.

[15] A. Ayazi, T. Baehr-Jones, Y. Liu, A. E.-J. Lim, and M. Hochberg, "Linearity of silicon ring modulators for analog optical links," *Opt. Exp.*, vol. 20, no. 12, pp. 13115–13122, Jun. 2012.

[16] L. Chen, J. Chen, J. Nagy, and R. M. Reano, "Highly linear ring modulator from hybrid silicon and lithium niobate," *Opt. Exp.*, vol. 23, no. 10, pp. 13255–13264, May 2015.

[17] C. Xiong *et al.*, "A linear push-pull silicon optical modulator," in *Proc. Frontiers Opt.*, 2014, Paper FM3A. 4.

[18] A. Samani, V. Veerasubramanian, E. El-Fiky, D. Patel, and D. V. Plant, "A silicon photonic PAM-4 modulator based on dual-parallel Mach–Zehnder interferometers," *IEEE Photon. J.*, vol. 8, no. 1, Feb. 2016, Art. ID 7800610.